Climatic Change (2025) 178:30
https://doi.org/10.1007/s10584-025-03875-x

Anthropogenic forcing dominates changes in compound long-duration dry and heat extremes in China

Fengchun Ye[1] · Pinya Wang[1] · Yang Yang[1] · Lili Ren[2] · Jianping Tang[3] · Hong Liao[1]

Received: 25 December 2023 / Accepted: 26 January 2025 / Published online: 5 February 2025

Abstract
In the context of global warming, the adverse impacts of compound dry and heat extremes (CDHEs) on human societies, ecosystems, and economies surpass those of single drought or heat extremes. This study investigates the trends of CDHEs in China from 1961 to 2014, meticulously analyzing key indicators including frequency, duration, high-temperature intensity, and total number of days. Through model simulations from the Coupled Model Intercomparison Project Phase 6 (CMIP6), we attribute the changes in CDHEs to various external driving factors. We have also assessed the projected variations in CDHEs under the low, medium, and high emission scenarios of the Shared Socioeconomic Pathway (SSP1-2.6, SSP2-4.5, and SSP5-8.5). CDHEs in China are predominantly concentrated in northeastern, central, and eastern regions of China, with all four indicators of CDHEs exhibiting increasing trends in most regions of China over the past 54 years. The impacts of anthropogenic forcing dominate the changes in CDHEs over China, especially over the northwest and southwestern regions where anthropogenic forcing can increase the probability of the occurrences of CDHEs by 1.3 times (range 1.2–1.5). Up to 40% of the occurrence of CDHEs in China can be attributed to anthropogenic forcing. Moreover, the impacts of anthropogenic forcing on CDHEs are higher for the extreme ones identified with more strict thresholds than the moderate ones. In the future, under the three scenarios in CMIP6, the occurrences of CHDEs are projected to increase over most of China, with the most substantial increases under SSP5-8.5. The anthropogenic emissions are expected to exert the greatest impacts on CDHEs over parts of northwestern and southwestern China, accounting for more than 80% of projected CDHEs increases therein in the future under SSP5-8.5.

Keywords Compound dry and heat events · Detection and attribution · Anthropogenic impacts · Future projections

Extended author information available on the last page of the article

1 Introduction

Under the background of global warming, frequent extreme weather events have struck China, including heat waves, persistent droughts, and flooding, causing devastating consequences, such as economic losses and environmental damage (Wang et al. 2023; Wang et al. 2021a, b; Zhen Feng et al. 2013). Extreme dry and heat events tend to occur simultaneously due to similar atmospheric conditions (Vogel et al. 2020). In particular, compared with individual extreme droughts and hot events, compound droughts and hot extremes are more destructive and harmful to humans, animals, and crops (Lacetera 2019; Mehrabi and Ramankutty 2017). For instance, the compound drought and hot extremes that occur during the crop-growing season have a much more severe impact on food security than individual droughts and hot events (Lu et al. 2018). The physiological and behavioral characteristics of animals could be altered by the combination of extremely dry and hot conditions, and the interactions between extreme droughts and heat may also have an impact on the immune function of animals (Padda et al. 2021). Prolonged periods of arid and hot conditions, such as those that dominated Europe in 2018, can increase the likelihood of soil moisture droughts and wildfires and have enormously negative effects on agriculture and society (Manning et al. 2018; Yin et al. 2023). Along with the continued global warming, it is projected that substantial rises in the occurrences of individual droughts and hot extremes as well as compound drought and hot extremes will manifest across the majority of global land areas (Luca and Donat 2023).

China has been hit by severe occurrences of compound extremes of drought and heat events in the past few years (Sun et al. 2014). The destructive impacts and increased risk of the occurrences of compound drought and hot extremes under global warming have led to growing attention to their temporal and spatial variability (e.g., Li et al. 2022; Wu et al. 2022; Zhang et al. 2023). It is revealed that the frequency of compound drought and hot extreme have increased in most regions of China in the past several decades (Wu et al. 2019), and they are projected to be more frequent across most of China in the future, especially over eastern parts and the wet and dry transition zones of China where severe compound dry and hot events increase the probability of agricultural droughts (Wu et al. 2020; Kong et al. 2020). Yang et al. (2023) focused on the spatiotemporal variability of typical long-duration compound dry and hot extremes (CDHEs) and pointed out that CDHEs in the east-central and north-western regions of China have experienced a notable rise in frequency, length, and intensity in the past several decades. Furthermore, it is shown that both daytime and nighttime compound dry and hot events in China have increased dramatically under various land cover types, which heightened the risk of forest fires and the potential adverse effects on human health (Feng et al. 2021). It is also suggested that with the elevated levels of future warming, China will experience substantially increased impacts from the compound drought and hot extremes (Wu et al. 2021; Yang and Tang 2023).

The occurrences and variations of extreme weather events are inextricable from global warming. Many studies have attributed extreme drought events and heat wave events to anthropogenic forcing including greenhouse gases, aerosol and land use, etc. (e.g., Clarke et al. 2022; Li et al. 2020; Wang et al. 2021a, b). Qian et al (2024) revealed that the record-breaking heat wave in North China in June 2023 was dominated by anthropogenic climate change. They claimed that the intensity of the 2023-like three-day heat wave has significantly increased by at least 1.0 °C (range 0.8 °C–1.3 °C) due to anthropogenic climate change. Sun et al. (2022) found that the rising greenhouse gas emissions are the main driver of the observed average and extreme temperature increases in China in the past decades (Sun et al. 2022). Tan et al. (2022) showed that extreme drought in southeastern China in 2020 was associated with excessive emissions of industrial aerosols and biomass-burning aerosols. Anthropogenic warming increased the risk of not only individual climate extremes but also compound extreme weather events and the associated climate disasters (AghaKouchak et al. 2020; Zscheischler et al. 2018). The anthropogenic forcing was found to be the most important factor dominating summer drought and heat wave events in Northeast China from 1951 to 2014 (Li et al. 2020). Chiang et al. (2022) showed that the large increases in simultaneous warm and dry months across most of the globe are driven by increased anthropogenic emissions. However, most of the recent studies have focused on the detection and attribution of individual droughts and/or hot extremes while the variability of compound drought and hot extremes receive less attention. Previous works have examined the anthropogenic influence on compound drought and hot extremes primarily from a monthly and seasonal timescale using monthly precipitation and air temperatures (Wu et al. 2022; Zhang et al. 2022a, b). However, extreme hot and dry events can occur within a span of just a few days.

Here in this work, following Manning et al. (2019) and Yang et al. (2023), we focus on the compound long-duration dry and hot events (CDHEs) which are identified as the extended dry periods that co-occur with extreme temperatures (see Sect. 2) and investigate their spatial and temporal variability during 1961–2014. Besides, the phase 6 of the Coupled Model Intercomparison Project (CMIP6) model outputs are applied for the variations of CDHEs in the past five decades. Finally, the future changes in CDHEs are assessed with model simulations from the Scenario Model Intercomparison Project (ScenarioMIP) of CMIP6 under different scenarios. This paper is organized as follows: the second section contains the data and methods; the third section describes the results; and the fourth section includes conclusions and discussion.

2 Data and methods

2.1 Observations

The observational data used in this study is the Climate Change Research Centre of the Chinese Academy of Sciences (CRC) CN05.1 grid observation dataset, which is obtained by interpolating the observation data based on more than 2,400 stations provided by the China Meteorological Administration (CMA) using the anomaly approach and contains seven elements, including average temperature, precipitation, maximum temperature, minimum temperature, average wind speed, relative humidity, and evapotranspiration, with a spatial resolution of $0.25° \times 0.25°$, and the time scale is daily and monthly average. This dataset is widely used in validating climate models and detecting climate change and has potential applications in agriculture, hydrology, and ecology (Wu and Gao 2013). In this study, daily maximum temperature and daily precipitation in summertime from 1961 to 2014 are used.

2.2 CMIP6 multi-model simulations

To investigate the anthropogenic forcing influence on the CDHEs in China from 1961 to 2014, the historical simulations of daily precipitation and daily maximum temperatures driven by various forcings from the Detection and Attribution Model Intercomparison Project (DAMIP) in the CMIP6 are used for analysis (Table 1). The different forcings include ALL forcing (ALL), greenhouse gas forcing (GHG), aerosol forcing (AER), and natural forcing (NAT). ALL forcing means that the model is subjected to both anthropogenic forcing (greenhouse gases, aerosols, land use, etc.) and natural forcing (volcanic eruptions and solar radiation). Ten CMIP6 global climate models (GCMs) providing all these experiments are used in this study (Table 1). Moreover, the anthropogenic forcing is obtained by subtracting the natural forcing from the full forcing (ANT), and the other anthropogenic forcing apart from GHG (OA) is obtained by subtracting GHG from the anthropogenic forcing, which includes aerosol, land use, and ozone (Najafi et al. 2015). For the analysis of the historical period, the ensemble members r1i1p1f1, r2i1p1f1, and r3i1p1f1 for each model are utilized.

In addition, the future changes of CDHEs under different emission scenarios are projected based on 21 available CMIP6 global climate models (GCMs) with daily precipitation and temperature simulations from 2041 to 2094 (Table 2). We use three SSP scenarios from ScenarioMIP of CMIP6 by coupling different socioeconomic pathways and different climatic forcings, namely, SSP1-2.6, SSP2-4.5, and SSP5-8.5, representing a low, midlevel, and high anthropogenic emission scenario, respectively. The CDHE indicators for each model are calculated first, and then the multi-model ensemble mean is obtained for each of the four CDHE indicators. The multi-model ensemble mean (MME) is used for analyses and demonstration (MME indicates the average results for multiple-model ensemble members). For all ScenarioMIP models of CMIP6, we use only one ensemble member (typically r1i1p1f1) even when more runs are available for some of the models. Note that both observations and the model simulations are re-interpolated to a spatial resolution of 2° × 2° for consistency.

2.3 Identifications of CDHEs and the associated indices

Dry and heat extremes are usually defined in terms of percentile thresholds as those above a certain percentile of precipitation and temperature, e.g., the 95th percentile (Feng et al. 2020; Jones and Moberg 2003; Stocker 2014). Following Yang et al. (2023), in this work, we use the drought duration and temperature intensity to define the compound long-duration

Table 1 List of GCMs from DAMIP in CMIP6 driven by various forcings (ALL, NAT, GHG, AER)

Model	Institution /Nation	Resolution
ACCESS-CM2	CSIRO-ARCCSS/Australia	1.875° × 1.25°
ACCESS-ESM1-5		
BCC-CSM2-MR	BCC/China	1.125° × 1.125°
CanESM5	CCCma/Canada	2.8125° × 2.8125°
CNRM-CM6-1	CNRM-CERFACS/France	1.40625° × 1.40625°
E3SM-2–0	E3SM-Project/USA	1° × 1°
FGOALS-g3	CAS/China	2° × 2.25°
GFDL-ESM4	NOAA-GFDL/USA	1.25° × 1°
MIROC6	MIROC/Japan	1.40625° × 1.40625°
MRI-ESM2-0	MRI/Japan	1.125° × 1.125°

Table 2 List of GCMs under the three SSP scenarios from ScenarioMIP in CMIP6

Model	Institution /Nation	Resolution
ACCESS-CM2	CSIRO-ARCCSS/Australia	1.875° × 1.25°
ACCESS-ESM1-5		
BCC-CSM2-MR	BCC/China	1.125° × 1.125°
CAMS-CSM1-0	CAMS/China	1.125° × 1.125°
CanESM5	CCCma/Canada	2.8125° × 2.8125°
CMCC-ESM2	CMCC/ Italy	1.25° × 0.9375°
CNRM-CM6-1	CNRM-CERFACS/France	1.40625° × 1.40625°
CNRM-ESM2-1		
EC-Earth3	E3SM-Project/USA	1° × 1°
FGOALS-g3	CAS/China	2° × 2.25°
GFDL-ESM4	NOAA-GFDL/USA	1.25° × 1°
INM-CM4-8	INM/ Russia	2° × 1.5°
INM-CM5-0		
IPSL-CM6A-LR	IPSL/France	2.5° × 1.2587°
MIROC6	MIROC/Japan	1.40625° × 1.40625°
MPI-ESM1-2-LR	MPI-M/Germany	1.875° × 1.875°
MRI-ESM2-0	MRI/Japan	1.125° × 1.125°
NESM3	NUIST/China	1.875° × 1.875°
NorESM2-LM	NCC/Norway	1.25° × 0.9375°
NorESM2-MM		
TaiESM1	AS-RCEC/Taiwan	1.25° × 0.9375°

dry and hot events. The drought duration means the number of consecutive days with daily precipitation less than 1 mm and temperature intensity is the highest value of daily maximum temperature during each drought. At each grid, a CDHE is identified when both the duration and temperature intensity exceed their respective 95th percentile thresholds during the summers of 1961–2014. Each model from different forcing scenarios utilizes the threshold obtained from ALL forcing simulation to identify CDHEs. In addition, we focus on four indices to characterize CDHEs, including Count, Duration, Magnitude, and Total days (Todays). Specifically, Count means the total events of persistent CDHEs per year; Duration is defined as the average consecutive days of CDHEs per year; Magnitude indicates the average of the highest daily maximum temperatures during each drought process per year; Todays is the total number of days of CDHEs per year. Note that CDHEs are obtained for the summer months (June, July, and August). In this work, the Mann–Kendall trend test which is one of the widely used non-parametric tests (Qian et al. 2019), is employed to detect significant trends in the four extreme indices.

2.4 Attribution analysis

The contribution of anthropogenic contributions to the long-term changes in CDHEs is obtained by comparing the characteristics of CDHEs in model simulations with and without anthropogenic forcings (Zhai et al. 2018). In this work, we use probability ratio (PR)

(Fischer and Knutti 2015) and fraction of attributable risk (FAR) (Stott et al. 2004) to evaluate the impacts of anthropogenic forcings on the probability of CDHEs (Stott et al. 2016; Wu et al. 2022). The corresponding equation is as follows:

$$PR = \frac{p_1}{p_0} \tag{1}$$

$$FAR = 1 - \frac{p_0}{p_1} \tag{2}$$

where p_0 and p_1 are the probability of occurrence of the CDHE under natural forcing only and all full forcing including both anthropogenic and natural forcing, respectively. As in previous works (Zhang et al 2022a, b), the probability p0 and p1 of CDHEs for each grid is empirically defined as the occurrence days divided by the total days within the focus periods in the simulations under NAT forcing and ALL forcing, respectively. Consequently, the ratio PR is the ratio between the frequency of occurrences of CDHEs under NAT forcing and ALL forcing. And the FAR (1–1/PR) refers to the fraction of the CDHEs attributed to anthropogenic forcing. PR value is an indicator for the contribution of anthropogenic forcing to the long-term of CDHEs and PR > 1 means that anthropogenic forcings increase the probability of CDHEs. FAR value indicates the fraction of changes in CDHEs attributable to anthropogenic forcing (Fischer and Knutti 2015). FAR ranges from −1 to 1, and a FAR between 0 and 1 indicates that the fraction of CDHEs is attributed to anthropogenic forcings. We also assess the impacts of anthropogenic emissions on CDHEs in the future, where p0 and p1 denote the probability of CDHEs in the historical simulation under ALL forcing and future projections under the SSP scenarios (Zhou et al. 2021). And PR > 1 means that changes in anthropogenic emission increase the probability of CDHEs in the future. Bootstrap resampling method (1000 times) is used for estimating the uncertainties of PR.

2.5 Signal-to-noise ratio

The signal-to-noise ratio (SNR) is adopted as an indicator to measure the uncertainties of the CMIP6 models' ensemble, and the equation is:

$$SNR = {}^{\overline{X}}\!/_{\sigma} \tag{3}$$

where $\overline{X}$ and σ denote the mean and standard deviation of the samples, respectively. The larger the SNR value the more credible the signal is larger than the noise (Kim et al. 2019).

3 Results

3.1 Historical changes in CDHEs from 1961–2014

Figure 1 demonstrates the spatial distributions of the climatological mean of the four indices associated CDHEs in observation and MME under ALL forcing of CMIP6 from 1961 to 2014. Based on the spatial patterns of Count, we can see that CDHEs are mainly located

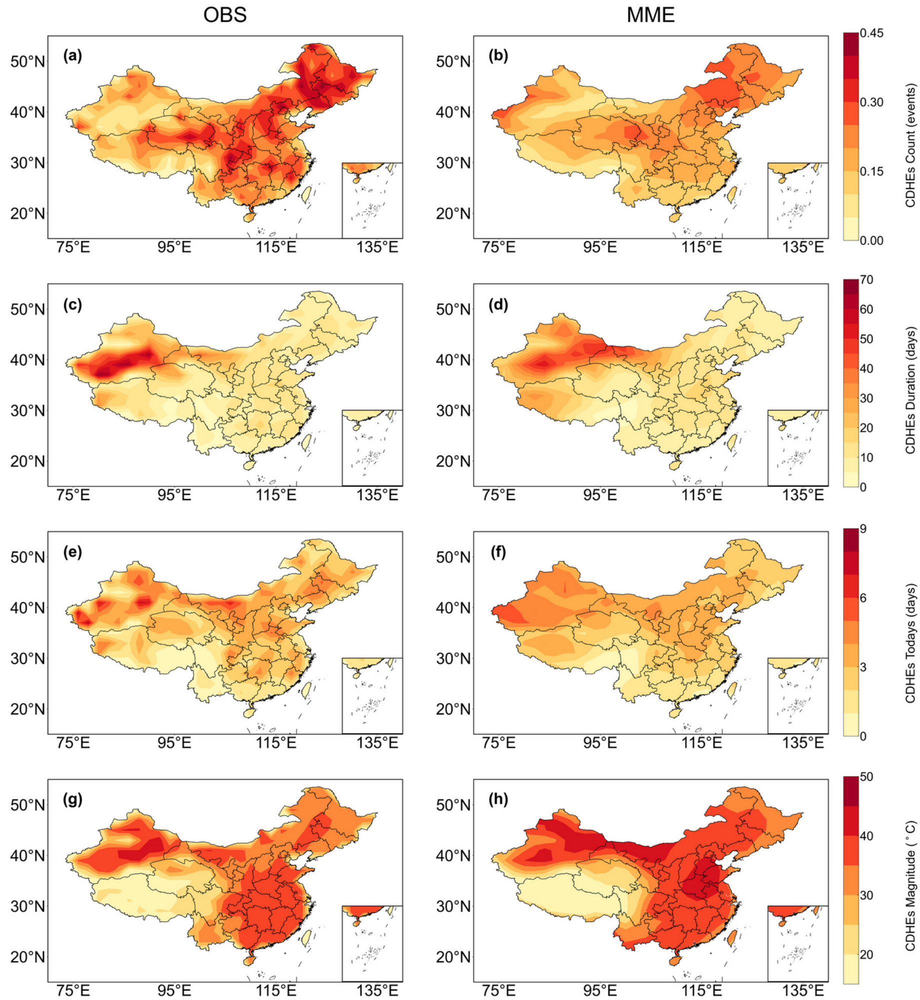

Fig. 1 Spatial distributions of averaged Count (**a** and **b**), Duration (**c** and **d**), Todays (**e** and **f**), and Magnitude (g&h) of CDHEs from 1961 to 2014. Panels on the left column for the observations and panels on the right column for the MME results under ALL forcing

over the northeastern, central, and eastern parts of China in observation, higher than those in MME with CDHEs mainly occurring in northwestern and northeastern China (Figs. 1a and b). The average Duration values of CDHEs are higher over northwestern China than the other regions in both observation and MME, with the maximum above 60 days (Figs. 1c and 2d). Determined by both Duration and Count, the Todays of CDHEs are relatively higher over northwestern and northern parts of China with a maximum above 8 days (Figs. 1e and f). The spatial pattern of the Magnitude of CDHEs in observation is similar to that in MME with higher values over northwestern, central, and eastern parts of China (Figs. 1g and h). In a word, the observed CDHE metrics are consistent with the MME results, exhibiting spatial correlations above 0.90. And these findings are generally consistent with the spatial distribution of the four indicators described in (Yang et al. 2023). Figure S3 demonstrates the

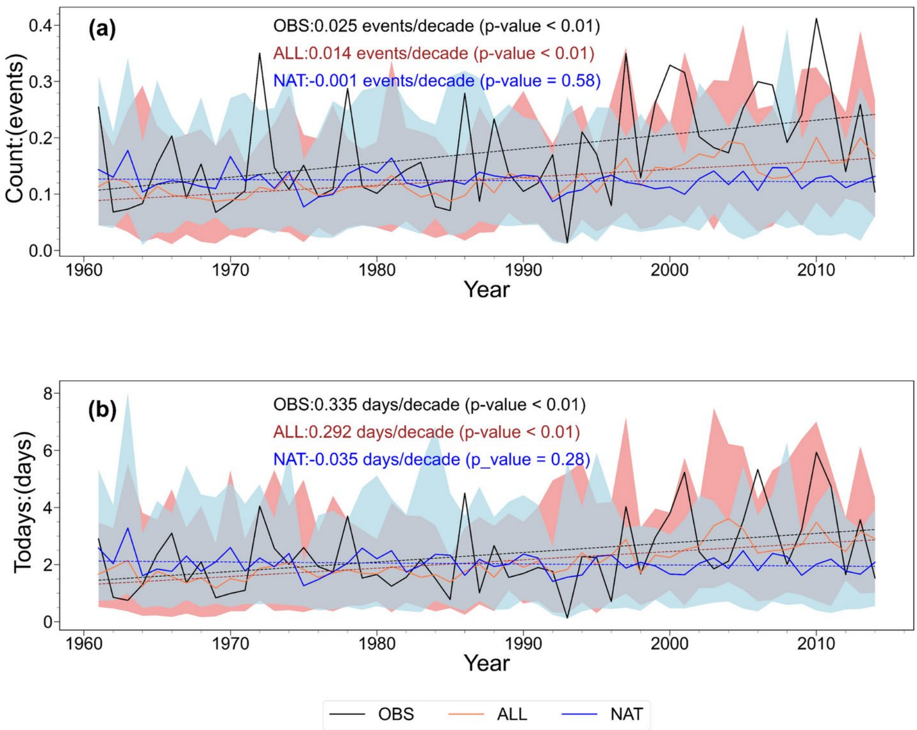

Fig. 2 Temporal series of observed and simulated area-weighted average of Count (**a**) and Todays (**b**) for China in multi-model simulations from CMIP6 under ALL and NAT forcing. The solid and dashed lines represent the time series and linear trends of the annual mean Count and Todays, respectively. The shading indicates the 5%–95% ranges for multi-model simulations

signal-to-noise ratio (SNR) values (Kim et al. 2019) for four metrics of CDHEs in CMIP6 simulations under ALL forcing. For all four metrics of CDHEs, the SNR values are larger than 1.0 over almost the whole China domain, with higher magnitudes over the eastern and northeastern parts of China, indicating relatively more robust simulations therein.

Figure 2 illustrates the annual variations of area-weighted averaged Count and Todays of CDHEs in China from 1961 to 2014 in both observations and MME of simulations under NAT and ALL forcing in CMIP6. The observed annual mean Count and Todays show obvious year-to-year variations and significant increasing trends (99% confidence level). The observed Count and Todays display a trend of 0.0025 events per year and 0.0335 days per year, respectively. It is clear that model simulations underestimate the observed Count and Todays under ALL forcing in CMIP6 though with a significant increasing trend. Moreover, the Root Mean Squared Error (RMSE) between the observed and simulated Count and Todays under ALL forcing is 0.04 and 0.69, apparently lower than those between simulations under NAT forcing and the observations. These findings indicate that anthropogenic influences play a substantial role in the increased trend in the Count and Todays of CDHEs.

To further understand the long-term change of CDHEs, the spatial distributions of the observed linear trends of the four indices associated with CDHEs in China from 1961 to 2014 are given in Fig. 3. As shown in Fig. 3a, the observed Count of CDHEs has increased

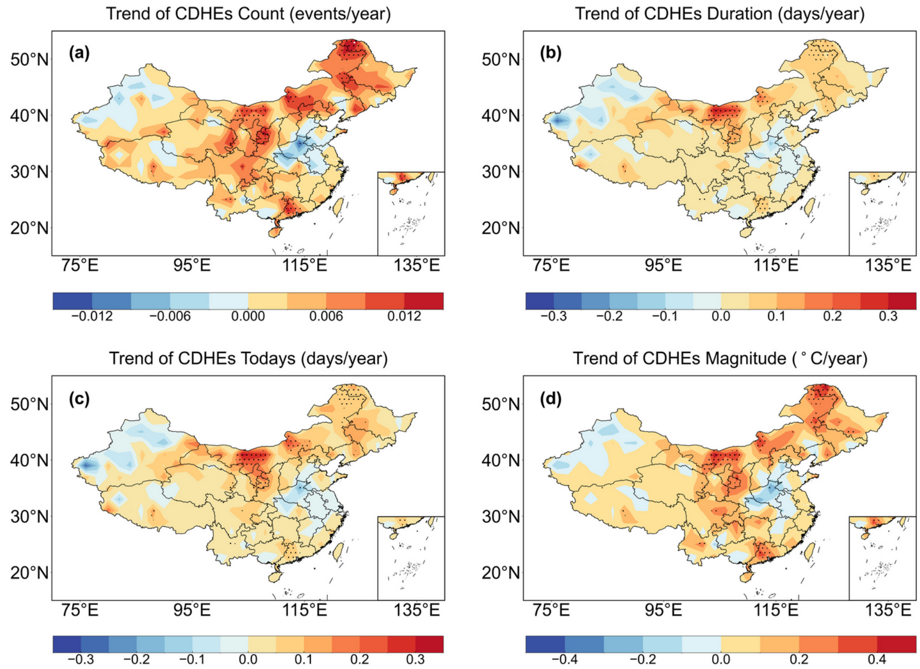

Fig. 3 Spatial distribution of the linear trends in the observations for the four indicators of CDHEs from 1961 to 2014. (**a**) Count, (**b**) Duration, (**c**) Todays, (**d**) Magnitude. The dotted areas pass the 95% confidence level of the Mann–Kendall test

in most regions of China in the past decades, with stronger increasing trends in the northeastern, northern, and southwestern parts of China while decreasing trends in the northwestern region and the central-eastern region of China. The other indices show similar spatial patterns that Duration, Todays, and Magnitude of CDHEs exhibit increasing trends in most of China, with significant trends observed over the Inner Mongolia region (Figs. 3b and c) and northeastern parts of China (Fig. 3d), but insignificant declining trends over central-eastern China. Therefore, the above results suggest that CDHEs in China have become more frequent, longer lasting, and stronger in the past five decades, and model simulations under ALL forcing can reasonably reproduce the spatial–temporal variability of observed long-term changes in CDHEs.

3.2 Attribution of the long-term changes in CDHEs

As strengthened above, anthropogenic forcing plays a substantial role in the long-term changes in difference indices of CDHEs. In this section, we further assess the contributions of different forcings to the changes in changes in CDHEs more explicitly. Figures 4, 5, 6 and 7 present the linear trends of the four indices associated with CDHEs under different forcings in MME of CMIP6. We can see that the linear trends of Count under ALL forcing in MME are generally consistent with the observations, with increasing trends over most of China, especially over northwestern, northern, and northeastern parts of China (Fig. 4a). The spatial pattern of linear trends for Count under ANT is consistent with that under ALL forc-

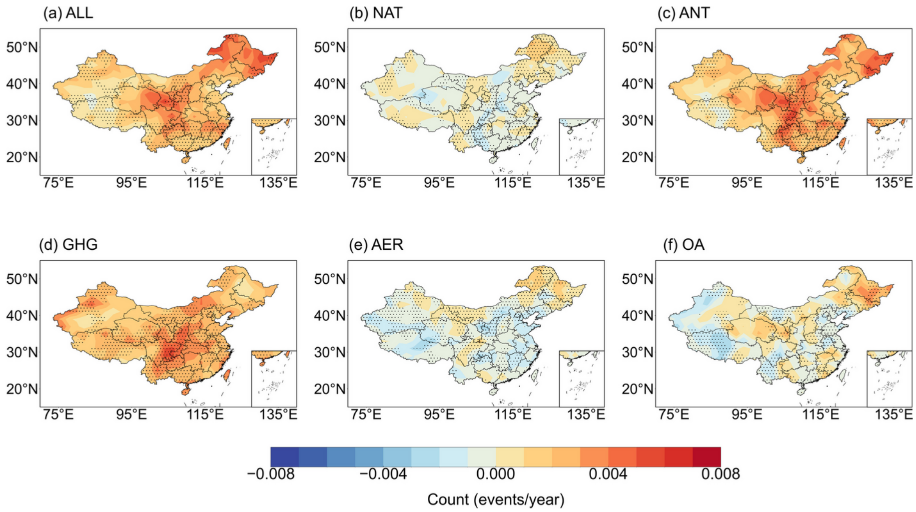

Fig. 4 Linear trends of Count in simulations under different forcings from 1961 to 2014. (**a**) ALL forcing, (**b**) NAT forcing, (**c**) ANT forcing, (**d**) GHG forcing, (**e**) AER forcing, (**f**) OA forcing. The dotted areas pass the 95% confidence level of the Mann–Kendall test

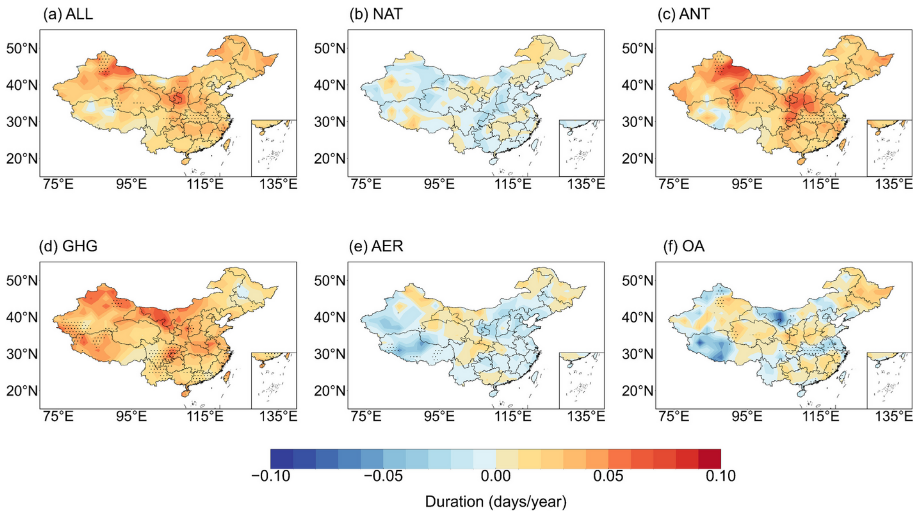

Fig. 5 Same as in Fig. 4 but for the linear trends of Duration

ing with increasing trends over most of China and comparable magnitudes (Fig. 4e) while the Count of CDHEs under NAT show a decreasing trend over most of China (Fig. 4b). Thus, anthropogenic forcing dominates the changes in Count of CDHEs in the past decades. Importantly, the impacts of GHG contribute the most to the changes in the Count of CDHEs with increasing trends over most of China (Fig. 4c), surpassing the impacts of AER and OA. The count of CDHEs under AER and OA shows weak increasing trends in central and northern China but negative trends in western China (Figs. 4d and f).

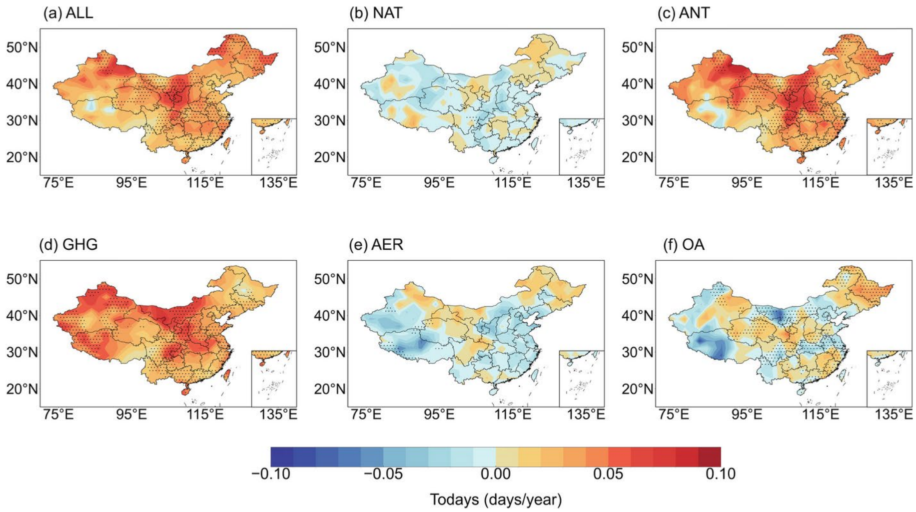

Fig. 6 Same as in Fig. 4 but for the Linear trends of Todays

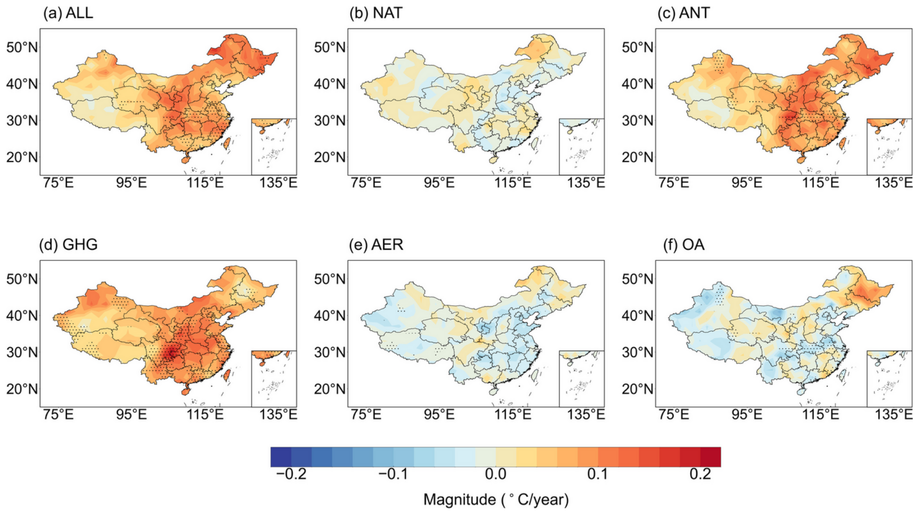

Fig. 7 Same as in Fig. 4 but for the linear trends of Magnitude under different forcings

The linear trends of Duration of CDHEs under ALL forcing show a similar spatial pattern to Count, with significant increasing trends over most of China, especially over northwestern, northeastern, and northern China (Fig. 5a). Similarly, ANT overtakes NAT, dominating the changes of Duration with increasing trends over most of China (Fig. 5e). Moreover, among GHG, AER, and OA, GHG contribute the most to changes in Duration with a positive trend covering most of China (Fig. 5c) while Duration under AER and OA exhibit a decreasing trend over most of China (Figs. 5b and f).

The Todays and Magnitude under ALL forcing show similar spatial patterns to Duration, exhibiting increasing trends over most of China, especially over northeastern and northern China, with magnitude above 0.1 days per year and 0.2 °C per year, respectively (Figs. 6a and 7a). Consistently, the increasing trends of Todays and Magnitude of CDHEs are also dominated by ANT (Figs. 6e and 7e) while Todays and Magnitude under NAT show weak increasing trends or decreasing trends across China (Figs. 6b and 7b). Besides, the effects of GHG overtake the impacts of AER and OA, contributing the most to the changes of Todays and Magnitude of CDHEs (Figs. 6c and 7c).

Particularly, Count, Todays, Duration, and Magnitude of CDHEs under AER show decreasing trends across most of China, suggesting that changes in aerosol levels in the past decades dampen the occurrences and inhibit their count, duration, frequency, and magnitude (Figs. 4d, 5d, 6d, and 7d). Note that the four indices of CDHEs under OA show weak positive trends in northeastern China, indicating that changes in land use and ozone concentrations can somewhat favor the occurrences of CDHEs (Figs. 4, 5, 6 and7f).

In summary, the simulations of MME under ALL, ANT, and GHG forcing can well capture the increasing trend of the four indices of CDHEs in observations, which confirms the substantial role of ANT, especially GHG in affecting the changes of CHDEs. In the following analysis, we quantitatively assess the impacts of anthropogenic forcing on CDHEs and examine the extent to which anthropogenic forcing influences CDHEs based on PR and FAR values. PR value indicates the extent to which anthropogenic forcing increases the probability of CDHEs occurring, and FAR value refers to the proportion of CDHEs that can be attributed to anthropogenic forcing.

Figure 8 gives the PR and FAR values for CDHEs during 1961–2014. Particularly, we consider CDHEs based on a lower and a higher threshold, i.e., the 75th and the 98th of Tmax and precipitation to assess the impacts of anthropogenic forcing on CDHEs at different criteria. For the current threshold (95th percentile), PR values exceed 1.0 over most of China, especially over southern and northwestern China, with the maximum above 1.6 (Fig. 8a). Accordingly, FAR values are positive over most of China, with the maximum above 0.4 over southern China and northwestern China (Fig. 8b). The results suggest that anthropogenic forcing could lead to 1.3 times increase in probability of CDHE occurrences in these regions, and 40% the occurrences of CDHEs can be attributed to anthropogenic factors forcing. The regional average of PR values across China for different thresholds are listed in Table S1(rows 1–3), with the 95% confidence intervals shown.

For CDHEs identified at a lower threshold of the 75th percentile, the spatial distributions of PR and FAR values are similar to those of the 95th percentile but with lower magnitude, with maximum values of PR and FAR values exceeding 1 and 0.2, respectively (Figs. 8c and d). This suggests that more than 20% of such CDHEs can be attributed to the influence of anthropogenic forcing. For CDHEs identified at a higher threshold of the 98th percentile, PR and FAR values are elevated over most of China, with PR value reaching 1.8 and FAR reaching 0.4 over northwestern and southeastern China. For CDHEs at the 98th percentile, the anthropogenic forcing generally causes a 1.6 times increase in the probability of CDHEs in southern and northwest China and more than 40% of CDHEs could be attributed to anthropogenic forcing effects therein. Therefore, anthropogenic forcing increased the probability of the occurrences of CDHEs and their increases from 1961 to 2014. Moreover, the impacts of anthropogenic forcing are higher for the extreme CDHEs identified with higher thresholds than the moderated ones.

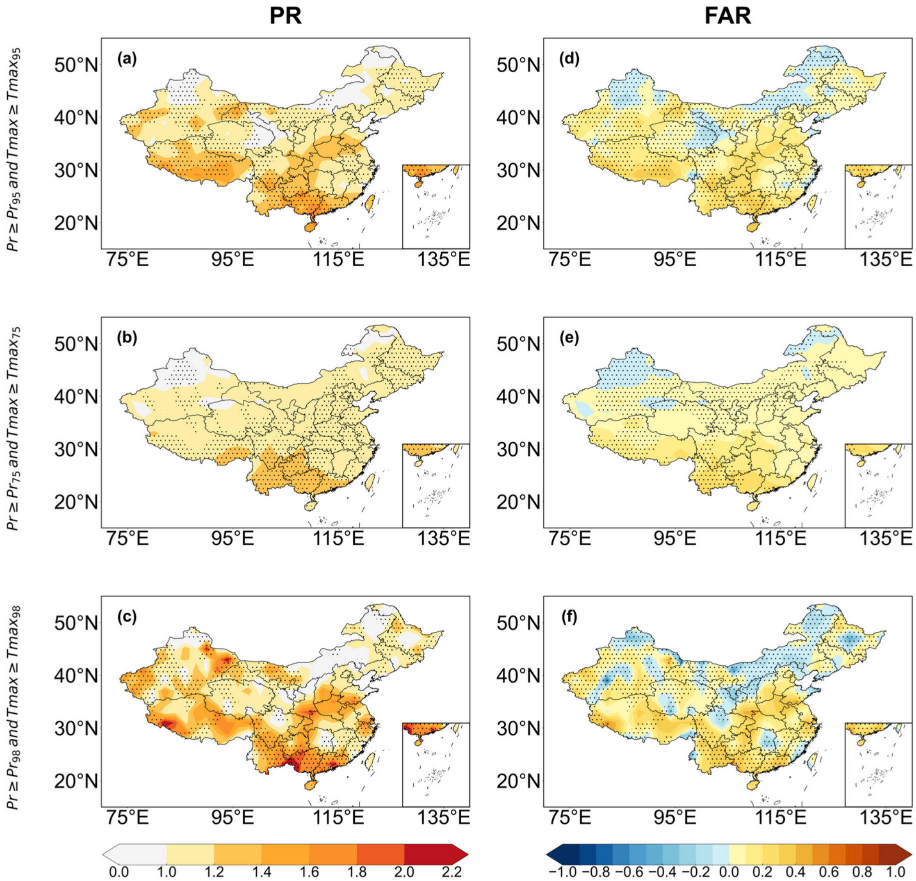

Fig. 8 PR (**a**, **b** and **c**) and FAR (**d**, **e** and **f**) values for CDHEs identified with the 95th, 75th, and 98th percentile thresholds of duration and temperature intensity under ALL forcing simulations relative to NAT forcing simulations from 1961 to 2014. The dotted areas pass the consistency test that more than half of the model simulations show the same sign

3.3 Future projections of CDHEs under difference scenarios

Figure 9 illustrates the future projected changes in the Count, Duration, Magnitude, and Todays of CDHEs across China for 2041–2094 (Fut) relative to the historical period of 1961–2014 (Hist) based on CMIP6 simulations across different scenarios, i.e., SSP1-2.6, SSP2-4.5 and SSP5-8.5. Across all three SSP scenarios, a notable surge in Count relative to Hist is projected across most regions in China (Figs. 9a, b and c). The spatial distributions of projected changes in the Count of CDHEs are similar with the most significant rise over the southwestern region, particularly along the Sichuan Basin, with an average increase of over 0.8 events per year for SSP1-2.6 (Figs. 9a). And the magnitude of changes in count are higher under the high emission scenario, with the maximum changes above 1.0 events/year under SSP5-8.5 (Figs. 9c). The Duration values of CDHEs are also projected to increase over most regions of China, especially over the northwestern part of China for the three scenarios (Figs. 9d, e and f). The average duration increases of CDHEs exceed 8 days per

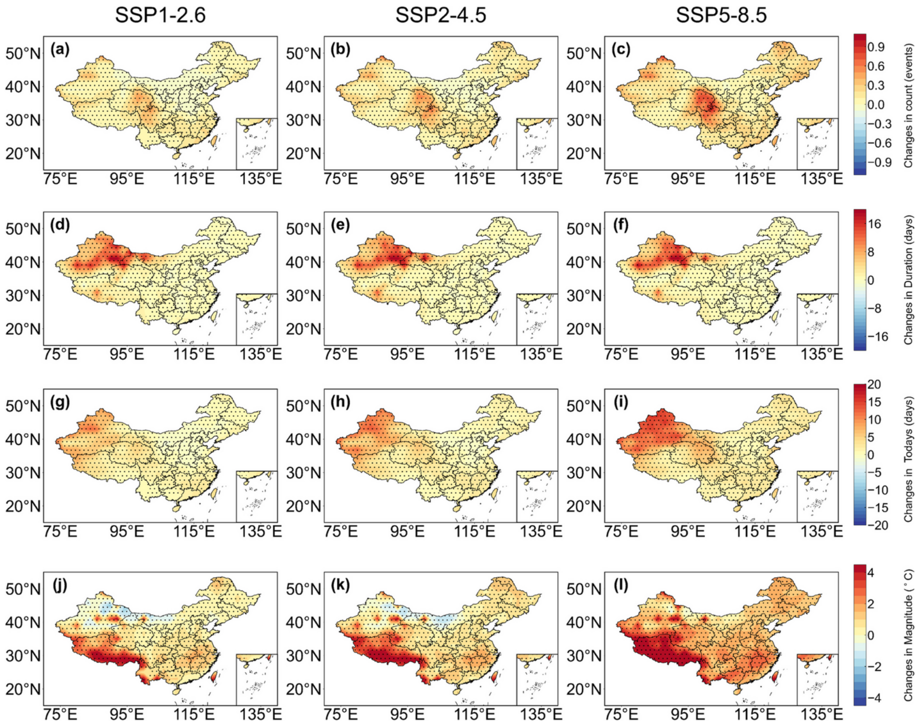

Fig. 9 Projected changes in the Count (**a**-**c**), Duration (**d**-**e**), Magnitude (**g**-**i**), and Todays (**j**-**l**) of CDHEs under SSP1-2.6, SSP2-4.5, and SSP5-8.5 scenarios from 2041 to 2094. Dots indicate that more than half of the models show the same sign

year over northwestern regions. The spatial patterns of future changes in Todays exhibits are similar to those of changes in Duration with higher magnitudes over the northwestern part of China (Figs. 9g, h, and i). In addition, the changes in Todays are highest under the highest forcing level of SSP5-8.5 with relatively higher increases over the northwestern and the central regions of China with maximum increases above 16 days per year compared to Hist, respectively (Figs. 9g, h and i). Consistently, the Magnitude values of CDHEs are projected to increase across all three SSP scenarios (Figs. 9j, k and l), with the maximum values above 3°C under SSP5-8.5 (Fig. 9l). In summary, the future changes in CDHEs in China suggest that CDHEs are projected to be more frequent, severe, and longer lasting in the future, especially under the high forcing level.

Figure 10 demonstrates the projected PR and FAR values from 2041 to 2094 under the three SSP scenarios. Here, to obtain PR values under different scenarios, p_0 and p_1 denote the probability of CDHE occurrences (Todays of CDHEs) in Hist and Fut, respectively. The PR indicates the extent to which the probability of CDHEs could be attributed to future emissions changes compared to the historical period. Meanwhile, the FAR values quantify the proportion of the amplified probability of CDHEs attributable to future changes in anthropogenic emissions. In the future period, the occurrence probability of CDHEs is higher relative to those under the historical period, with PR values higher than 2.0 over most of China especially over the northwestern part under all three SSP scenarios. The PR values

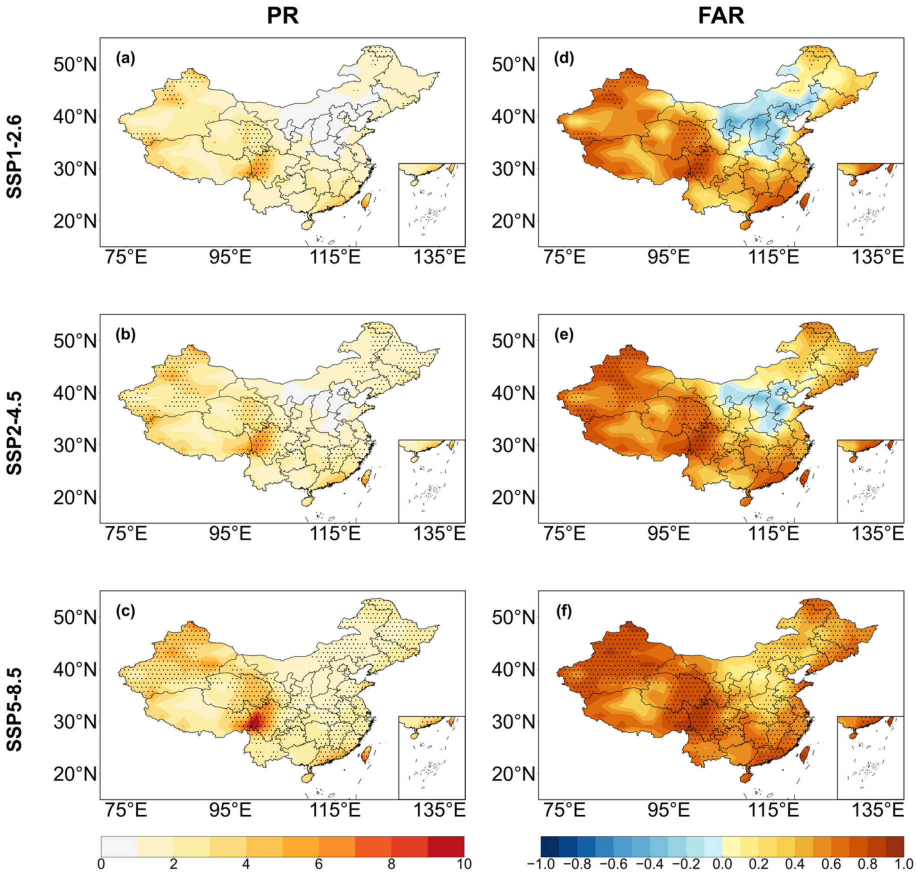

Fig. 10 PR and FAR values for CDHEs during 2041–2094 relative to the Hist period under the SSP1-2.6, SSP2-4.5, and SSP5-8.5 scenario, respectively. The dotted areas indicate more than half of the models show the same sign

are the highest under the highest forcing level under SSP5-8.5, with PR values above 4 over northwestern and part of southwestern China (Fig. 10c). Moreover, positive FAR values cover most of China under the three SSP scenarios (Figs. 10d, e and f), and the impacts are stronger under SSP2-4.5 and SSP5-8.5 compared to the relatively lower forcing under SSP1-2.6. Specifically, FAR values are greater than 0.4, 0.6, and 0.8 over most of China under SSP1-2.6, SSP2-4.5, and SSP5-8.5, respectively. This indicates that anthropogenic forcing accounts for more than 60% and 80% of CDHEs increases over most of China in the future under SSP2-4.5 and SSP5-8.5. Note that under SSP1-2.6 and SSP2-4.5, the PR values in the North China Plain are less than 1, indicating that the occurrences of CDHEs therein could be mitigated under the future low and medium emission scenarios. The regional average of PR values across China under different scenarios are given in Table S1 (rows 4–6). Therefore, the rising anthropogenic emissions lead to more frequent CDHEs in the future, especially under the higher emission pathway. And the control of anthropogenic emissions is an effective approach to mitigating extreme weather events.

4 Conclusion and discussions

In this study, we investigate the spatiotemporal characteristics of CDHEs from different aspects based on the observed dataset of CN05.1 and assess the anthropogenic impacts on the historical and future projected changes of CDHEs through CMIP6 simulations. The observations show that the higher Count values of CDHEs are mostly found in the northwest of China. The spatial distribution of Duration, Todays, and Magnitude is similar to that of Count, with the highest values mostly found in the northwest, central, and eastern regions. Moreover, the four indicators of CDHEs exhibit a significant increase in most regions of China, particularly in the eastern and some northwestern areas. Furthermore, the MME results of historical simulations under the ALL forcing can effectively replicate the observed increasing trends of these four indicators of CDHEs.

Based on CMIP6 simulations under ALL forcing, NAT forcing, AER forcing, and GHG forcing, we quantify the impact of anthropogenic forcing on CDHEs. It is found that more than 40% of CDHEs in southern and northwestern parts of China are attributable to anthropogenic forcing, and the changes in greenhouse gases dominate the impacts of anthropogenic forcing. Specifically, anthropogenic impacts increase the probability of CDHEs by 1.3 times for CDHEs during 1961–2014. In addition, we assess the impacts of anthropogenic forcing on CDHEs identified with different thresholds, i.e., the 75th, 95th, and 98th of temperature and precipitation, and we find that the anthropogenic forcing plays a more important role for the more extreme CDHEs with a higher threshold than the moderated ones. Lastly, we analyze the future projected changes in CDHEs based on CMIP6 simulations under three different SSP scenarios (SSP1-2.6, SSP2-4.5, and SSP5-8.5). Results suggest that CDHEs will get more frequent, longer lasting, and stronger across most of China in the future relative to the historical period, especially for the high emission scenario SSP5-8.5. In addition, the impacts of emission changes on increases in CDHEs are elevated relative to the Hist period, especially over the northwestern and southwestern regions of China. Under the low and medium emission scenarios (SSP1-2.6 and SSP2-4.5), the occurrences of CDHEs over North China Plain could be mitigated compared with the historical period, which deserves further attention.

In this work, we use the PR and FAR indices to quantify the effects of anthropogenic forcing on CDHEs. It should be noted that the relatively coarse resolution of CMIP6 simulations may have affected the analysis of CDHEs on the regional scale (Di Luca et al. 2020), the dynamical downscaling simulations with a regional climate model may be effective for improving the results (Tang et al. 2016). The future projected climate is influenced by both anthropogenic forcing and internal variability. Following Cheng et al. (2015) and Wu et al. (2020), We applied a multiple linear regression model to obtain the respective contributions of the precipitation and temperature variability to the trends of the Count, Duration, Todays and Magnitude (See Text S1). Changes in precipitation trends have a greater impact on the four indicators of CDHEs in southeastern China, while changes in temperature trends exert a greater influence in northwestern China. The maximum contributions from changes in precipitation and temperature trends can exceed 80% (Figs. S1 and S2). As stressed by Bevacqua et al. (2022), the trends of precipitation play a pivotal role in the projected CDHEs. The Coordinated Regional Climate Downscaling Experiment (CORDEX) was initiated under the auspices of the World Climate Research Program (WCRP) to enhance downscaling techniques and their application in understanding and assessing regional climate change. Currently, it continues with the dynamical downscaling of global climate projections from

CMIP6. Higher resolution models or downscaling techniques could be employed in the future to provide more accurate regional predictions. Moreover, how the uncertainty of the internal variability affects CDHEs deserves further investigation.

Supplementary Information The online version contains supplementary material available at https://doi.org/10.1007/s10584-025-03875-x.

Author's contributions Fengchun Ye performed the data analysis, visualization, and wrote the manuscript. Pinya Wang and Yang Yang contributed to the study conception, data collection, and editing. All authors commented on previous versions of the manuscript. Lili Ren reviewed the manuscript, and helped perform the analysis with constructive discussions. All authors read and approved the final manuscript.

Funding This research was supported by the National Natural Science Foundation of China (42105166, 42475032, and 42293323), the Natural Science Foundation of Jiangsu Province (BK20241902), and the Jiangsu Science Fund for Carbon Neutrality (BK20220031).

Data availability The CMIP6 model result are accessible https://esgf-node.llnl.gov/projects/cmip6.

Declarations

Conflicts of interest The authors have no conflicts of interest to declare that are relevant to the content of this article.

References

AghaKouchak A, Chiang F, Huning LS, Love CA, Mallakpour I, Mazdiyasni O, Moftakhari H, Papalexiou SM, Ragno E, Sadegh M (2020) Climate extremes and compound hazards in a warming world. Annu Rev Earth Planet Sci 48:519–548. https://doi.org/10.1146/annurev-earth-071719-055228

Bevacqua E, Zappa G, Lehner F, Zscheischler J (2022) Precipitation trends determine future occurrences of compound hot–dry events. Nat Clim Chang 12(4):350–355. https://doi.org/10.1038/s41558-022-01309-5

Cheng S, Guan X, Huang J, Ji F, Guo R (2015) Long-term trend and variability of soil moisture over East Asia. J Geophys Res: Atmosp 120(17):8658–8670. https://doi.org/10.1002/2015JD023206

Chiang F, Greve P, Mazdiyasni O, Wada Y, AghaKouchak A (2022) Intensified likelihood of concurrent warm and dry months attributed to anthropogenic climate change. Water Resour Res 58(6):e2021WR030411. https://doi.org/10.1029/2021WR030411

Clarke B, Otto F, Stuart Smith R, Harrington L (2022) Extreme weather impacts of climate change: An attribution perspective. Environ Res: Clim 1(1):012001. https://doi.org/10.1088/2752-5295/ac6e7d

De Luca P, Donat MG (2023) Projected changes in hot, dry, and compound hot-dry extremes over global land regions. Geophys Res Lett 50(13):e2022GL102493. https://doi.org/10.1029/2022GL102493

Di Luca A, Pitman AJ, de Elía R (2020) Decomposing temperature extremes errors in CMIP5 and CMIP6 models. Geophys Res Lett 47(14):e2020GL088031. https://doi.org/10.1029/2020GL088031

Feng S, Hao Z, Wu X, Zhang X, Hao F (2021) A multi-index evaluation of changes in compound dry and hot events of global maize areas. J Hydrol 602:126728. https://doi.org/10.1016/j.jhydrol.2021.126728

Feng S, Wu X, Hao Z, Hao Y, Zhang X, Hao F (2020) A database for characteristics and variations of global compound dry and hot events. Weather Clim Extremes 30:100299. https://doi.org/10.1016/j.wace.2020.100299

Fischer EM, Knutti R (2015) Anthropogenic contribution to global occurrence of heavy-precipitation and high-temperature extremes. Nat Clim Chang 5(6):560–564. https://doi.org/10.1038/nclimate2617

Jones PD, Moberg A (2003) Hemispheric and large-scale surface air temperature variations: an extensive revision and an update to 2001. J Clim 16(2):206–223. https://doi.org/10.1175/1520-0442(2003)016%3c0206:HALSSA%3e2.0.CO;2

Kim I, Oh J, Woo S, Kripalani RH (2019) Evaluation of precipitation extremes over the Asian domain: observation and modeling studies. Clim Dyn 52(3–4):1317–1342. https://doi.org/10.1007/s00382-018-4193-4

Kong Q, Guerreiro SB, Blenkinsop S, Li XF, Fowler HJ (2020) Increases in summertime concurrent drought and heatwave in Eastern China. Weather Clim Extremes 28:100242. https://doi.org/10.1016/j.wace.2019.100242

Lacetera N (2019) Impact of climate change on animal health and welfare. Anim Front 9(1):26–31. https://doi.org/10.1093/af/vfy030
Li H, Chen H, Sun B, Wang H, Sun J (2020) A detectable anthropogenic shift toward intensified summer hot drought events over Northeastern China. Earth Space Sci 7(1):e2019EA000836. https://doi.org/10.1029/2019EA000836
Li W, Jiang Z, Li LZX, Luo JJ, Zhai P (2022) Detection and attribution of changes in summer compound hot and dry events over northeastern china with CMIP6 models. J Meteorol Res 36(1):37–48. https://doi.org/10.1007/s13351-022-1112-8
Lu Y, Hu H, Li C, Tian F (2018) Increasing compound events of extreme hot and dry days during growing seasons of wheat and maize in China. Sci Rep 8(1):16700. https://doi.org/10.1038/s41598-018-34215-y
Manning C, Widmann M, Bevacqua E, Loon AFV, Maraun D, Vrac M (2018) Soil Moisture drought in Europe: a compound event of precipitation and potential evapotranspiration on multiple time scales. J Hydrometeorol 19(8):1255–1271. https://doi.org/10.1175/JHM-D-18-0017.1
Manning C, Widmann M, Bevacqua E, Van Loon AF, Maraun D, Vrac M (2019) Increased probability of compound long-duration dry and hot events in Europe during summer (1950–2013). Environ Res Lett 14(9):094006. https://doi.org/10.1088/1748-9326/ab23bf
Mehrabi Z, Ramankutty N (2017) The cost of heat waves and droughts for global crop production. bioRxiv 188151. https://doi.org/10.1101/188151
Najafi MR, Zwiers FW, Gillett NP (2015) Attribution of Arctic temperature change to greenhouse-gas and aerosol influences. Nat Clim Chang 5(3):246–249. https://doi.org/10.1038/nclimate2524
Padda SS, Glass JR, Stahlschmidt ZR (2021) When it's hot and dry: Life-history strategy influences the effects of heat waves and water limitation. J Exp Biol 224(7):jeb236398. https://doi.org/10.1242/jeb.236398
Qian C, Ye Y, Jiang J, Zhong Y, Zhang Y, Pinto I, Huang C, Li S, Wei K (2024) Rapid attribution of the record-breaking heatwave event in North China in June 2023 and future risks. Environ Res Lett 19(1):014028. https://doi.org/10.1088/1748-9326/ad0dd9
Qian C, Zhang XB, Zhen L (2019) Linear trends in temperature extremes in China, with an emphasis on non-Gaussian and serially dependent characteristics. Clim Dyn 53:533–550. https://doi.org/10.1007/s00382-018-4600-x
Stocker T (2014) Climate change 2013: The physical science basis: working group i contribution to the fifth assessment report of the intergovernmental panel on climate change. Cambridge University Press
Stott PA, Christidis N, Otto FEL, Sun Y, Vanderlinden JP, van Oldenborgh GJ, Vautard R, von Storch H, Walton P, Yiou P, Zwiers FW (2016) Attribution of extreme weather and climate-related events. Wires Clim Change 7(1):23–41. https://doi.org/10.1002/wcc.380
Stott PA, Stone DA, Allen MR (2004) Human contribution to the European heatwave of 2003. Nature 432(7017):610–614. https://doi.org/10.1038/nature03089
Sun Y, Zhang X, Ding Y, Chen D, Qin D, Zhai P (2022) Understanding human influence on climate change in China. National Science Review 9(3):nwab113. https://doi.org/10.1093/nsr/nwab113
Sun Y, Zhang X, Zwiers FW, Song L, Wan H, Hu T, Yin H, Ren G (2014) Rapid increase in the risk of extreme summer heat in Eastern China. Nat Clim Chang 4(12):1082–1085. https://doi.org/10.1038/nclimate2410
Tang J, Niu X, Wang S, Gao H, Wang X, Wu J (2016) Statistical downscaling and dynamical downscaling of regional climate in China: Present climate evaluations and future climate projections. J Geophys Res: Atmosp 121(5):2110–2129. https://doi.org/10.1002/2015JD023977
Tan X, Wu X, Huang Z, Deng S, Hu M, Yew Gan T (2022) Detection and attribution of the decreasing precipitation and extreme drought 2020 in southeastern China. J Hydrol 610:127996. https://doi.org/10.1016/j.jhydrol.2022.127996
Vogel MM, Hauser M, Seneviratne SI (2020) Projected changes in hot, dry and wet extreme events' clusters in CMIP6 multi-model ensemble. Environ Res Lett 15(9):094021. https://doi.org/10.1088/1748-9326/ab90a7
Wang L, Sun L, Li W, Chen X, Li Y, Zou X, Jiang Y (2023) State of China's climate in 2022. Atmosp Ocean Sci Lett 16(6):100356. https://doi.org/10.1016/j.aosl.2023.100356
Wang S, Huang J, Yuan X (2021) Attribution of 2019 extreme spring-early summer hot drought over Yunnan in Southwestern China. Bull Am Meteor Soc 102(1):S91–S96. https://doi.org/10.1175/BAMS-D-20-0121.1
Wang W, Zhang Y, Guo B, Ji M, Xu Y (2021) Compound droughts and heat waves over the Huai River Basin of China: from a perspective of the magnitude index. J Hydrometeorol 22(11):3107–3119. https://doi.org/10.1175/JHM-D-20-0305.1
Wu J, Gao XJ (2013) A gridded daily observation dataset over China region and comparison with the other datasets. Chin J Geophys 56(4):1102–1111. https://doi.org/10.6038/cjg20130406
Wu X, Hao Z, Hao F, Li C, Zhang X (2019) Spatial and temporal variations of compound droughts and hot extremes in China. Atmosphere 10(2):95 https://doi.org/10.3390/atmos10020095
Wu X, Hao Z, Tang Q, Zhang X, Feng S, Hao F (2021) Population exposure to compound dry and hot events in China under 1.5 and 2°C global warming. Int J Climatol 41(12):5766–5775. https://doi.org/10.1002/joc.7152

Wu X, Hao Z, Zhang X, Li C, Hao F (2020) Evaluation of severity changes of compound dry and hot events in China based on a multivariate multi-index approach. J Hydrol 583:124580. https://doi.org/10.1016/j.jhydrol.2020.124580
Wu X, Hao Z, Zhang Y, Zhang X, Hao F (2022) Anthropogenic influence on compound dry and hot events in China based on Coupled Model Intercomparison Project Phase 6 models. Int J Climatol 42(8):4379–4390. https://doi.org/10.1002/joc.7473
Yang Y, Maraun D, Ossó A, Tang J (2023) Increased spatial extent and likelihood of compound long-duration dry and hot events in China, 1961–2014. Nat Hazard 23(2):693–709. https://doi.org/10.5194/nhess-23-693-2023
Yang Y, Tang J (2023) Substantial differences in compound long-duration dry and hot events over China between transient and stabilized warmer worlds at 1.5°C global warming. Earth's Futur 11(3):94. https://doi.org/10.1029/2022EF002994
Yin J, Gentine P, Slater L, Gu L, Pokhrel Y, Hanasaki N, Guo S, Xiong L, Schlenker W (2023) Future socio-ecosystem productivity threatened by compound drought–heatwave events. Nat Sustain 6(3):259–272. https://doi.org/10.1038/s41893-022-01024-1
Zhai P, Zhou B, Chen Y (2018) A review of climate change attribution studies. J Meteorol Res 32(5):671–692. https://doi.org/10.1007/s13351-018-8041-6
Zhang G, Wang H, Gan TY, Zhang S, Shi L, Zhao J, Su X, Song S (2022) Climate change determines future population exposure to summertime compound dry and hot events. Earth's Future 10(11):e2022EF003015. https://doi.org/10.1029/2022EF003015
Zhang Y, Hao Z, Zhang X, Hao F (2022) Anthropogenically forced increases in compound dry and hot events at the global and continental scales. Environ Res Lett 17(2):024018. https://doi.org/10.1088/1748-9326/ac43e0
Zhang Y, Hao Z, Zhang Y (2023) Agricultural risk assessment of compound dry and hot events in China. Agric Water Manag 277:108128. https://doi.org/10.1016/j.agwat.2022.108128
Zhen Feng M, Jia L, Shun Qian Z, Wen Xiu C, Shu Qun Y (2013) Observed climate changes in Southwest China during 1961–2010. Adv Clim Chang Res 4(1):30–40. https://doi.org/10.3724/SP.J.1248.2013.030
Zhou T, Ren L, Zhang W (2021) Anthropogenic influence on extreme Meiyu rainfall in 2020 and its future risk. Sci China Earth Sci 64(10):1633–1644. https://doi.org/10.1007/s11430-020-9771-8
Zscheischler J, Westra S, van den Hurk BJJM, Seneviratne SI, Ward PJ, Pitman A, AghaKouchak A, Bresch DN, Leonard M, Wahl T, Zhang X (2018) Future climate risk from compound events. Nat Clim Chang 8(6):469–477. https://doi.org/10.1038/s41558-018-0156-3

Authors and Affiliations

Fengchun Ye[1] · Pinya Wang[1] · Yang Yang[1] · Lili Ren[2] · Jianping Tang[3] · Hong Liao[1]

✉ Pinya Wang
pinya.wang@nuist.edu.cn

✉ Yang Yang
yang.yang@nuist.edu.cn

[1] Jiangsu Key Laboratory of Atmospheric Environment Monitoring and Pollution, Control, Jiangsu Collaborative Innovation Center of Atmospheric Environment and Equipment Technology, Joint International Research Laboratory of Climate and Environment Change, School of Environmental Science and Engineering, Nanjing, University of Information Science and Technology, Nanjing, Jiangsu, China

[2] College of Environment and Ecology, Jiangsu Open University, Nanjing, Jiangsu, China

[3] School of Atmospheric Sciences, Nanjing University, Nanjing, Jiangsu, China